Supporting Information

N_2-plasma-rapidly-engineered NiFe-LDH surfaces into an ultrathin FeOOH overlayer for highly durable seawater oxidation

Zhipeng Chen[a,e†], Lin Chen[a†], Shiqi Yin [a], Yuning Zhang[a], Yao Ding[d], Kaicai Fan[a], Lingbo Zong[a], Lei Wang[a], Xiaofan Du[b,c,*], Zhiqiang Hu[a,*] and Tianrong Zhan[a,*]

[a] Key Laboratory of Optic-electric Sensing and Analytical Chemistry for Life Science (Ministry of Education), College of Chemistry and Molecular Engineering, State Key Laboratory of Advanced Optical Polymer and Manufacturing Technology, Qingdao University of Science and Technology, Qingdao 266042, China

[b] Qingdao Industrial Energy Storage Research Institute, Qingdao Institute of Bioenergy and Bioprocess Technology, Chinese Academy of Sciences, Qingdao 266101, China

[c] Shandong Energy Institute, Qingdao, 266101, China

[d] Binzhou Polytechnic, Binzhou, 256603, China

[e] *Befar Group Co., Ltd,* Binzhou*, 256600, China*

[*] Corresponding author, Tel & Fax: +86-532-84023927
E-mail address: trzhan@qust.edu.cn (T. Zhan), duxf@qibebt.ac.cn (X. Du), huzhiqiang@qust.edu.cn (Z. Hu).
[†] These authors contributed to the work equally and should be regarded as co-first authors.

Chemicals and materials

Ni foam (NF, porosity: 99.8%, PPI: 110) was purchased from Shengernuo Technology Co. Ltd. KOH (≥ 85%), NaCl (≥ 99.5%), $Ni(NO_3)_2 \cdot 6H_2O$ (≥ 98%), $Fe(NO_3)_3 \cdot 9H_2O$ (≥ 98%), HCl (36.0~38.0%), urea (≥ 99%), and ethanol (≥ 99.7%) were obtained from Sinopharm Chemical Reagent Co., Ltd. Ultrapure water with resistivity ≥ 18.25 MΩ cm^{-1} was used in all experiments. All reagents were of analytical grade and were used directly as received.

Materials characterizations

The phase structures were analyzed by X-ray diffraction patterns (XRD, Rigaku Miniflex 600 powder diffractometer, λ=1.54050 Å, 40 kV, and 100 mA, Japan) at a scan rate of 5º min^{-1} in a range of 5º ~ 80º. The morphologies were evaluated by scanning electron microscope (SEM, TESCAN MIRA LMS, Czech Republic), transmission electron microscopy (TEM), and high-resolution TEM (HRTEM, JEM-F200, Japan JEOL). Elemental states and compositions were characterized by X-ray photoelectron spectroscopy (XPS) on an HP 5950A ESCA spectrometer with a MgKa source. The obtained binding energy was corrected to 284.9 eV at C 1s. Ex and In-situ Raman measurements were performed using a Laser Raman Spectrometer (Invia Qontor, England Renishaw) at an excitation wavelength of 532 nm. Inductively coupled plasma-optical emission spectroscopy (ICP-OES, Agilent 5110) was used to quantify the amount of Ni and Fe in the LDH samples. The specific surface area was calculated from N_2 adsorption-desorption isotherms measured at 77 K using a surface area and porosity analyzer (BET, Micromeritics ASAP 2460). Prior to measurement, the samples were degassed under vacuum at 120 °C for 6 h. The BET surface area was derived from the adsorption data in the relative pressure (P/P_0) range of 0.05 – 0.30. The O vacancies were analyzed by electron paramagnetic resonance (EPR) on an instrument of Bruker A300 Germany.

Electrochemical Measurements

Electrochemical tests were carried out on an electrochemical workstation (CHI 660E) with a three-electrode system at room temperature. Hg/HgO was used as the reference electrode, while a graphite rod was used as the counter electrode for OER. The prepared samples (size of 1 cm × 1 cm) were directly used as working electrodes. The LSV curves were collected at a scan rate of 5 mV s^{-1} with 85 % iR correction in 1 M KOH, alkaline seawater (1 M KOH + seawater), and alkaline simulated seawater (1 M KOH + 0.5 M NaCl) electrolytes after at least 30-cycle cyclic voltammetry

(CV) scanning to reach a stable. Electrochemical impedance spectroscopy (EIS) was measured in a frequency range of 100 kHz to 0.1 Hz at the open circuit potential with an amplitude of 5 mV. Potentials were converted to the reversible hydrogen electrode (RHE) with the equation $E_{RHE} = E_{Hg/HgO} + 0.059 \times pH + 0.098$ V. The long-term stability measurement was assessed by the chronopotential method. The corresponding Tafel plots were obtained by fitting the LSV curves between the overpotential (η) and log current density (log j) via the equation $\eta = b \log j + a$, where b is the Tafel slope. The corrosion polarization test was carried out under an open circuit potential (OCP) to measure the corrosion potential (E_{corr}) and corrosion current (I_{corr}) of NiFe-LDH/FeOOH and NiFe-LDH in different electrolytes. To estimate double-layer capacitances (C_{dl}), the CV curves were performed in the non-Faradaic region (1.073 ~ 1.173 V vs. RHE) at different scan rates of 30, 70, 110, 150, and 190 mV s^{-1}. The electrochemically active surface area (ECSA) was determined by the C_{dl}. By plotting the capacitive current against the scan rates, the C_{dl} was obtained as half of the corresponding slope value, and then the ECSA was derived from the equation: $ECSA = C_{dl}/C_s$, in which C_s is the specific capacitance for a flat surface (40 μF cm^{-2}).

TOF calculations: The surface concentration of Ni active sites (Γ, mol/cm^2) was calculated using the equation: $Slope = (n^2F^2A\Gamma) / (4RT)$, where n is the number of electrons transferred during the oxidation of Ni^{2+} to Ni^{3+} (n=1), F is the Faraday constant, A is the geometrical area of the electrode (1 cm^2), R and T represent the universal gas constant and absolute temperature, respectively. The slope was obtained from the linear regression of the oxidation current responses versus scan rate. The number of moles of Ni on the surface participating in the OER, denoted as m, was calculated using the equation: $m = A * \Gamma$. Finally, the TOF was calculated using the equation: $TOF = jA / (4Fm)$, where j is the current density (A/cm^2) of the catalysts at a fixed overpotential, and 4 represents the four-electron transfer process involved in the OER.

Density Functional Theory (DFT) Calculations

First-principle DFT calculations in the present study are performed using the Vienna ab initio Simulation (VASP)[1, 2] within the MedeA® computational environment. The valence electron and core ion interaction are described by the projector augmented wave (PAW) method[3]. The electron exchange-correlation interaction is approximately described by the generalized gradient approximation (GGA) with Perdew-Burke-Ernzerhof (PBE) function[4]. The electronic wave functions are represented by a plane wave basis with a cutoff energy of 500 eV. In addition, to

describe the van der Waals (vdW) interactions of graphite, the semiempirical dispersion potential (DFT-D3) was used. All structures in the calculations are explored using PBE + U, with an effective Ueff = U-J term of 5.5 and 5.0 eV, for the Ni and Fe 3d states. The structure relaxation was considered completed with the conjugate gradient method when a force convergence criterion was less than 0.02 eV $Å^{-1}$ and total energy convergence within 1×10^{-4} eV per unit cell. The Brillouin zone was sampled at the r mesh, and the Gaussian smearing method with a smearing width of 0.2 eV are used. For the density of states (DOS) and band structure calculations, a 4×4×4 Monkhorst-Pack k-mesh is used, and the Gaussian smearing method with a smearing width of 0.02 eV is used.

MD simulations.

Molecular dynamics (MD) simulations were performed to study the anion distributions close to the electrode surfaces. In the simulation box, the mixed solution model of NaCl aqueous solution was placed on the electrode surface. For comparison, both NiFe-LDH and NiFe-LDH-FeOOH heterostructures are considered as the electrodes. A vacuum layer with a thickness of about 35 Å was added above the solution to exclude interactions between the neighboring images, corresponding to the box size of ca. 15Å × 23 Å × 65 Å. All the atoms in the electrode model were fixed, and the particles in the solution model were free. An external electric field of 0.10 V/Å was applied along the z direction. Dynamics simulations were performed for 5 ns for equilibration and 10 ns for trajectory analysis under the NVT ensemble at 300 K. At least 5 trajectories were collected to reduce the random error. All the MD simulations were carried out using the LAMMPS software package.[5]

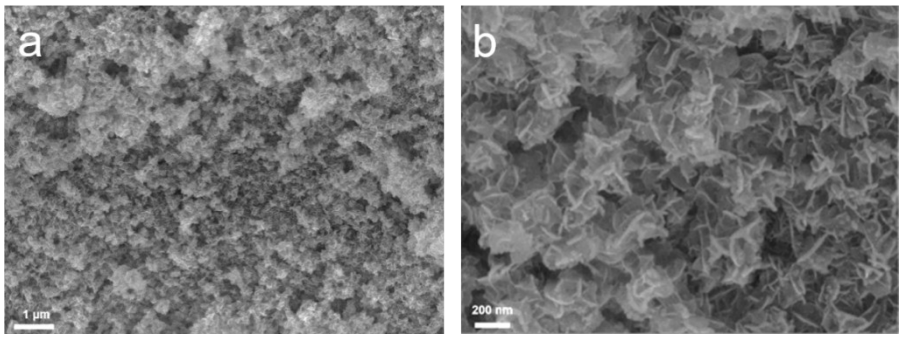

Fig. S1. (a, b) SEM images of NiFe-LDH.

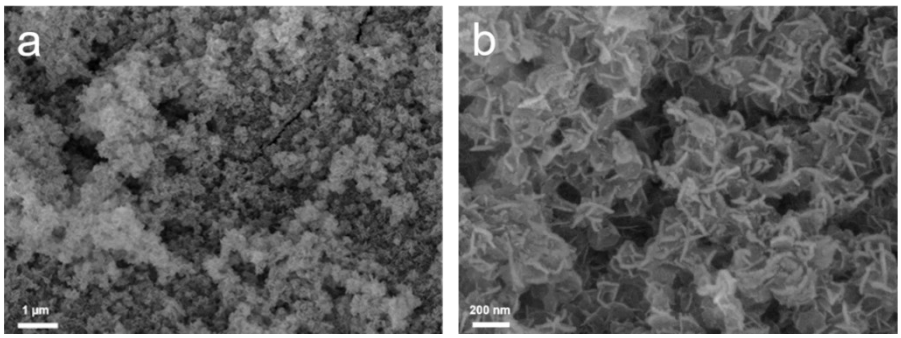

Fig. S2. (a, b) SEM images of NiFe-LDH/FeOOH.

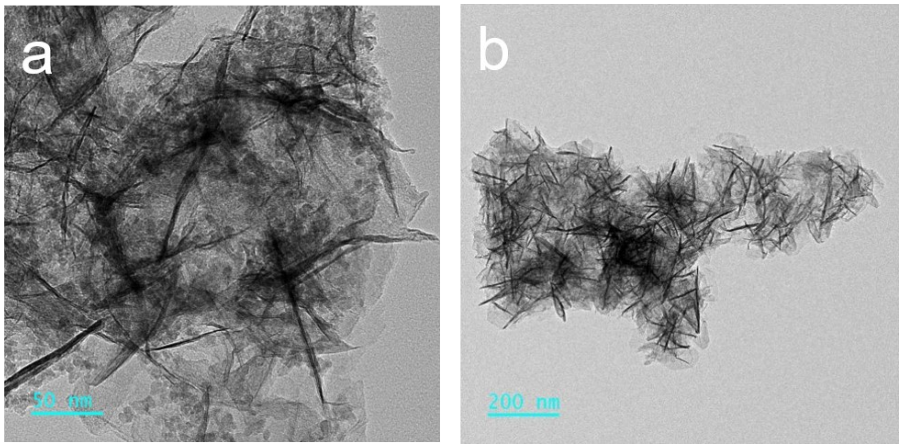

Fig. S3. (a, b) TEM images of NiFe-LDH/FeOOH.

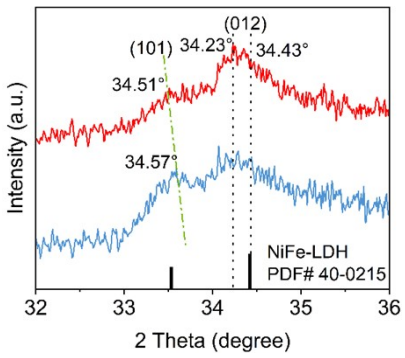

Fig. S4. XRD patterns of NiFe-LDH/FeOOH and NiFe-LDH.

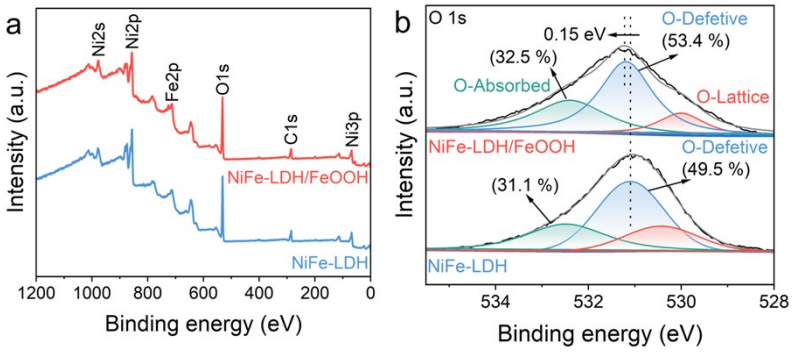

Fig. S5. (a) XPS survey, and (b) O 1s spectra of NiFe-LDH/FeOOH and NiFe-LDH.

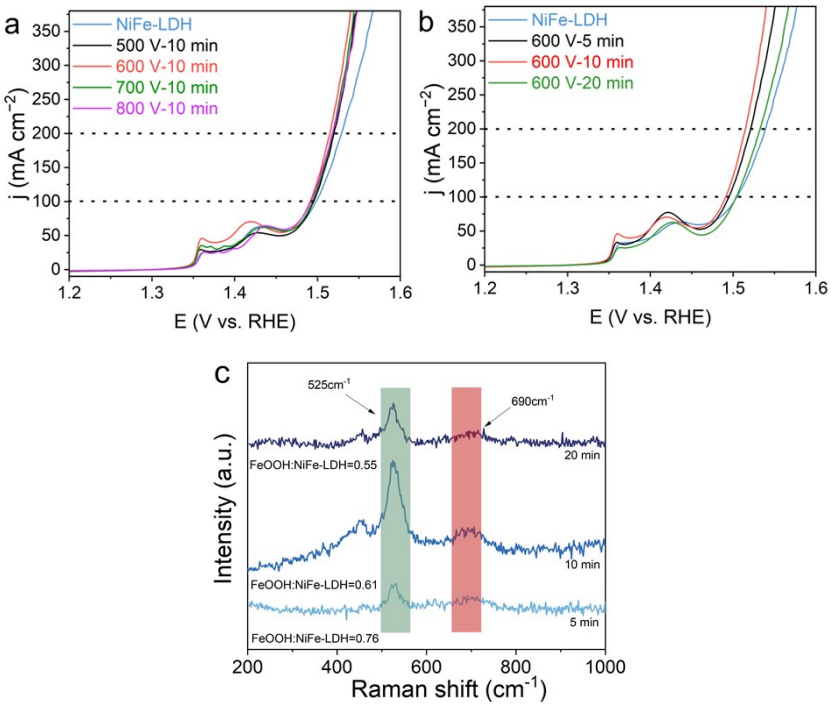

Fig. S6. OER LSV curves and Tafel plots of NiFe-LDH after the treatment of the N_2-plasma under different (a) applied voltages and (b) processing durations. The electrolyte is 1 M KOH + 0.5 M NaCl. (c) Raman spectra of NiFe-LDH after the different durations of the N_2-plasma for 5, 10, and 20 min.

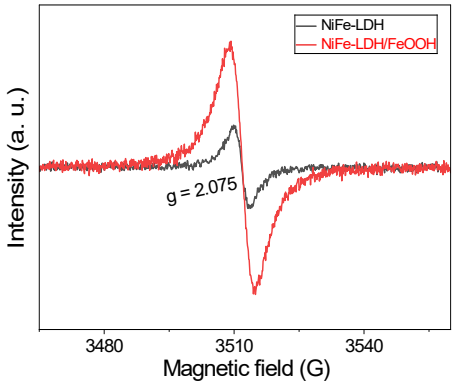

Fig. S7. EPR spectra of NiFe-LDH and NiFe-LDH/FeOOH.

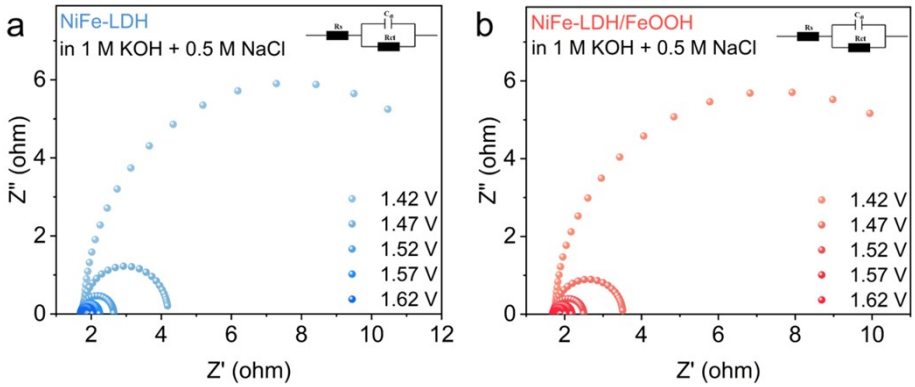

Fig. S8. Nyquist plots for (a) NiFe-LDH and (b) NiFe-LDH/FeOOH at different applied potentials versus RHE in 1 M KOH + 0.5 M NaCl electrolyte.

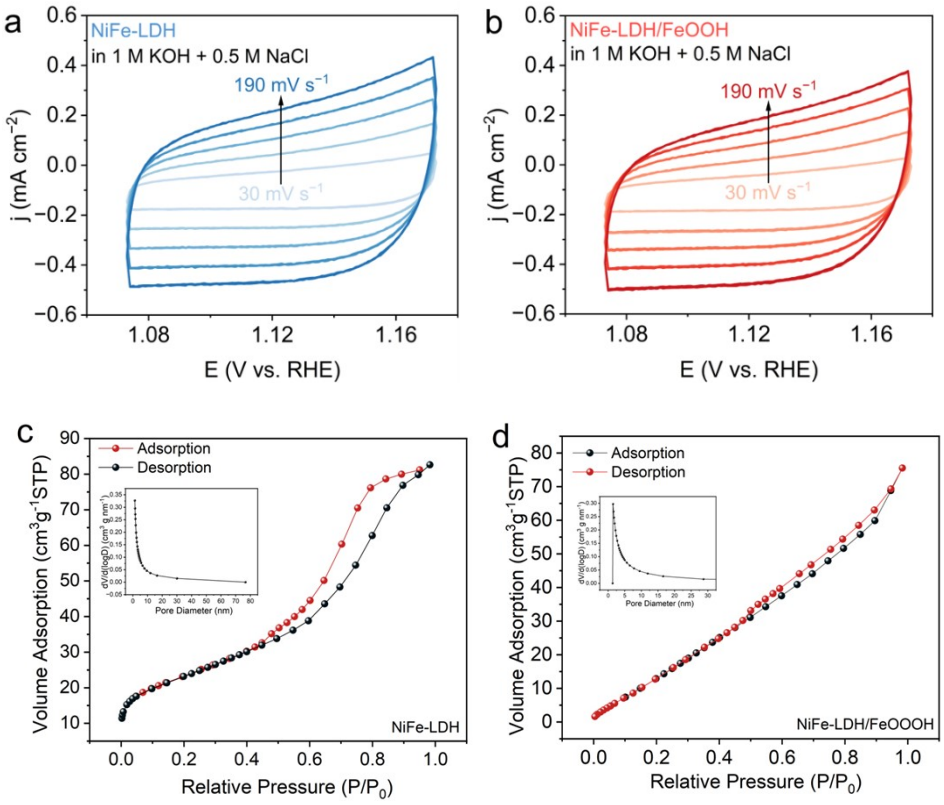

Fig. S9. CV curves of (a) NiFe-LDH, (b) NiFe-LDH/FeOOH at different scan rates for OER under the potential from 1.073 V to 1.173 V vs. RHE in 1 M KOH + 0.5 M NaCl electrolyte. N_2 adsorption-desorption curve of (c) NiFe-LDH and (d) NiFe-LDH/FeOOH.

Note. As shown in Fig. S8c-S8d, the both catalysts exhibit characteristic mesoporous structures. Specifically, the NiFe-LDH/FeOOH composite shows a Type V isotherm, possessing a specific surface area of 83.155 m^2/g and a total pore volume of 0.1232 cm^3/g. In comparison, the NiFe-LDH material displays a Type IV isotherm with a BET specific surface area of 91.639 m^2/g and a total pore volume of 0.1168 cm^3/g. The slightly decreased surface area is aligned with the ECSA result. Nonetheless, the OER activity and the ECSA-normalized activity of NiFe-LDH/FeOOH are better than those of NiFe-LDH (Fig. 3a and 3i). This observation further corroborates that the N_2-plasma-induced-formed FeOOH overlayer can improve the intrinsic OER activity of NiFe-LDH. This can be ascribed to the heterostructure owing to the introduction of the ultrathin FeOOH overlayer. Although some surface sites of NiFe-LDH are physically covered, the interfacial electronic structure are effectively optimized through the strong interfacial electronic interaction, thereby endowing catalytic centers with higher intrinsic activity.

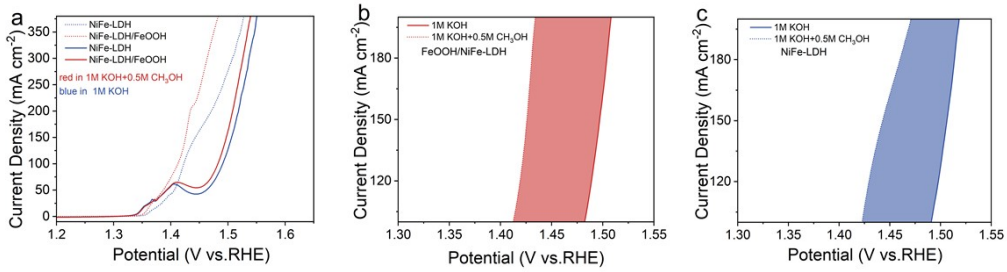

Fig. S10. LSV curves of NiFe-LDH/FeOOH and NiFe-LDH in 1 M KOH and 1 M KOH + CH_3OH.

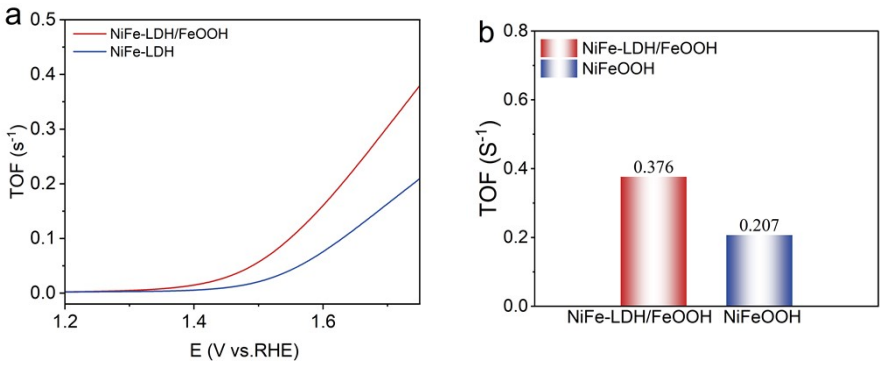

Fig. S11. TOF of NiFe-LDH/FeOOH and NiFe-LDH in a 1 M KOH + 0.5 M NaCl electrolyte.

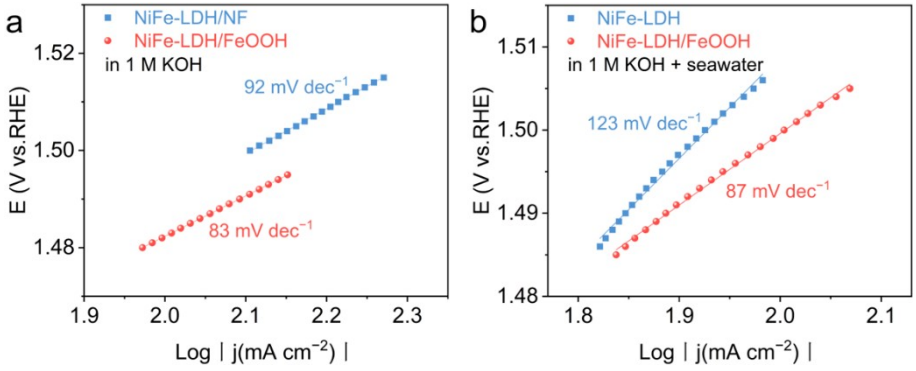

Fig. S12. Tafel plots of NiFe-LDH and NiFe-LDH/FeOOH in (a) 1 M KOH and (b) 1 M KOH + seawater electrolytes.

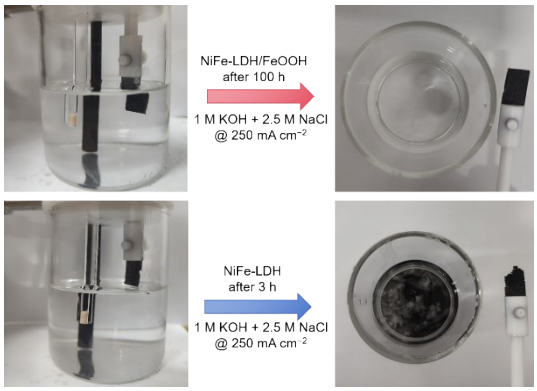

Fig. S13. The state of NiFe-LDH/FeOOH and NiFe-LDH under different corrosion times.

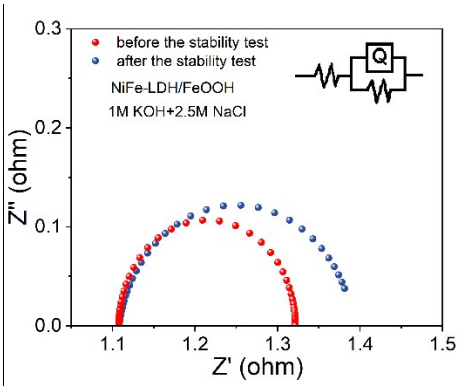

Fig. S14. EIS plots of NiFe-LDH/FeOOH before and after the durability test at 250 mA cm^{-2} in the 1 M KOH + 2.5 M NaCl electrolyte.

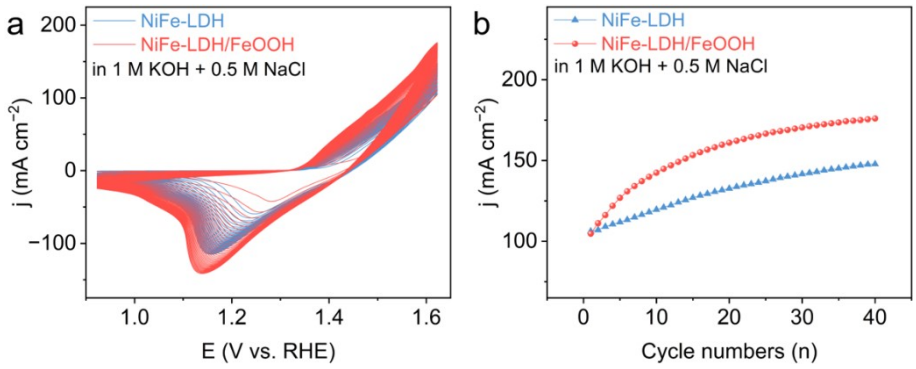

Fig. S15. (a) 40 CV cycles in the potential range of 0.923−1.623 V versus RHE at a scan rate of 100 mV s^{-1}. (b) Comparison of the current densities with the increase of CV cycles at a potential of 1.623 V vs. RHE.

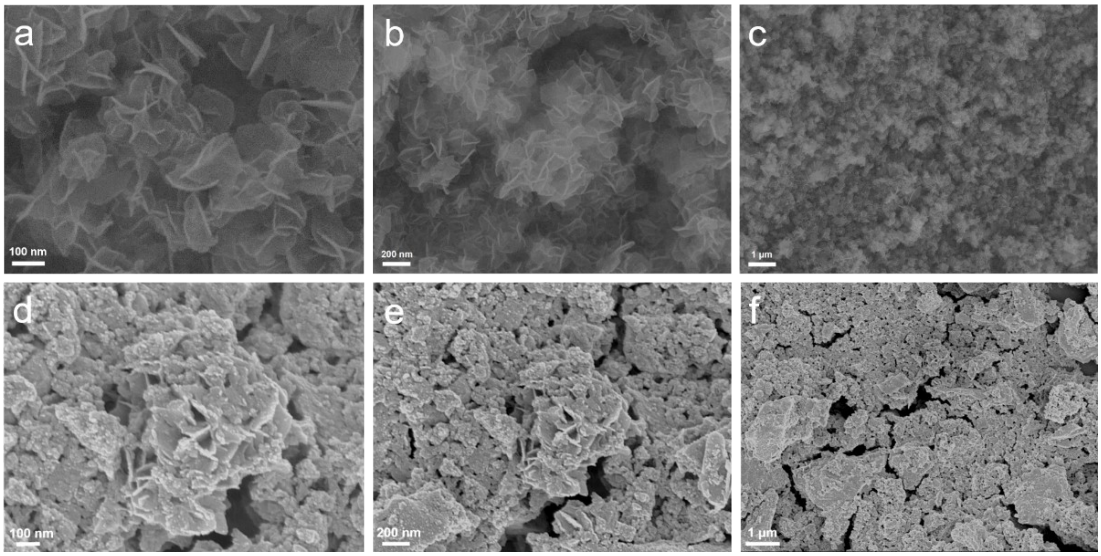

Fig. S16. SEM image of (a-c) NiFe-LDH/FeOOH and (d-f) NiFe-LDH after OER test in 1 M KOH + 2.5 M NaCl solution.

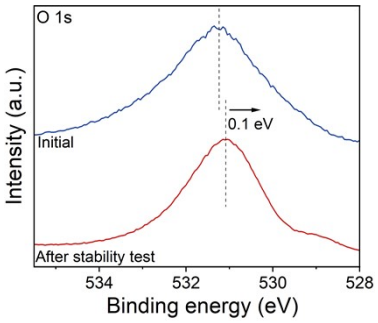

Fig. S17. O 1s XPS spectra of the used NiFe-LDH/FeOOH sample after CP stability test in 1 M KOH + 2.5 M NaCl electrolyte.

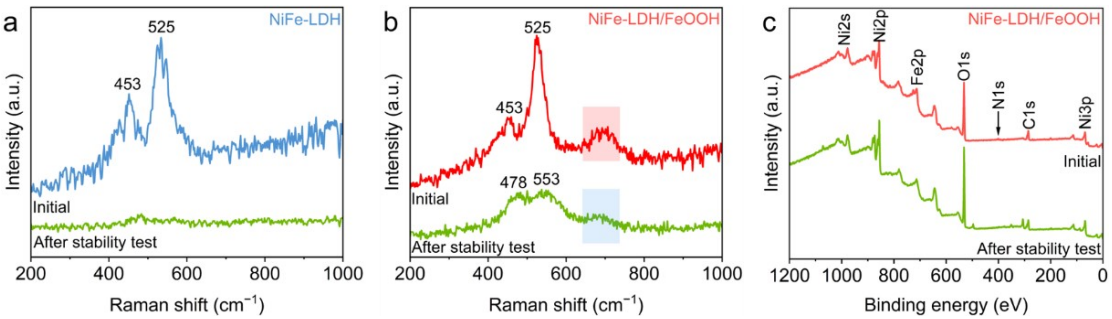

Fig. S18. Raman spectra of (a) NiFe-LDH and (b) NiFe-LDH/FeOOH before and after the OER test in 1 M KOH + 2.5 M NaCl solution. (c) XPS survey spectra of NiFe-LDH/FeOOH before and after the OER test in 1 M KOH + 2.5 M NaCl solution.

Fig. S19. Photos of KI starch paper reacting with the electrolyte (1 M KOH + 2.5 M NaCl) after a CP test for 3 hours on NiFe-LDH/FeOOH (left) and NiFe-LDH (right) at 250 mA cm^{-2}.

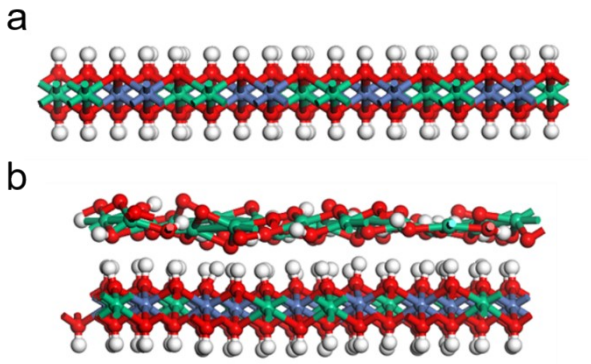

Fig. S20. Theoretical models of (a) NiFe-LDH and (b) NiFe-LDH/FeOOH. The blue, green, white, and red balls represent Ni, Fe, H, and O, respectively.

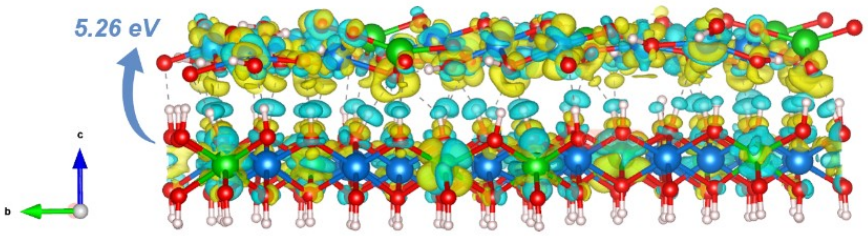

Fig. S21. Differential charge density diagram of NiFe-LDH/FeOOH (The blue and yellow colors indicate the decrease and increase of the electron density, respectively.).

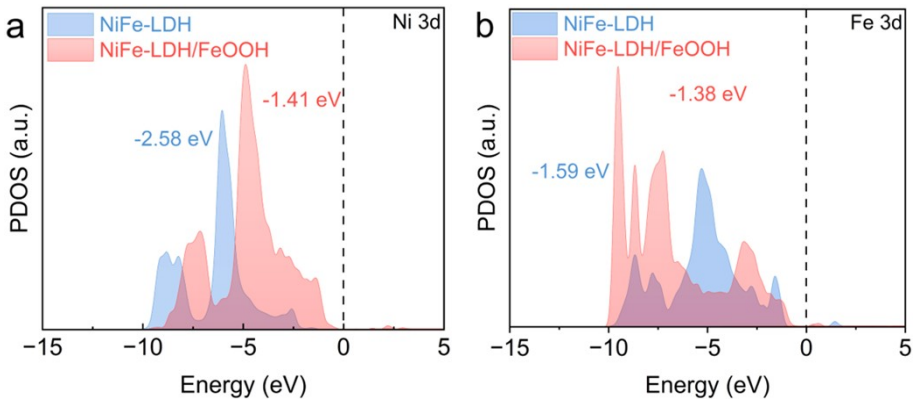

Fig. S22. The partial density of states (PDOS) of (a) Ni and (b) Fe 3d orbitals over NiFe-LDH/FeOOH and NiFe-LDH.

Table S1. Ni 2p XPS fitting of NiFe-LDH and NiFe-LDH/FeOOH.

Catalysts	Peak	Position (eV)	Area
NiFe-LDH	Ni^{3+} $2p_{1/2}$	874.7	10596
	Ni^{2+} $2p_{1/2}$	873.3	10284
	Ni^{3+} $2p_{3/2}$	856.9	19427
	Ni^{2+} $2p_{3/2}$	855.6	24571
NiFe-LDH/FeOOH	Ni^{3+} $2p_{1/2}$	874.6	8296
	Ni^{2+} $2p_{1/2}$	873.3	7291
	Ni^{3+} $2p_{3/2}$	856.7	17073
	Ni^{2+} $2p_{3/2}$	855.6	17660

Table S2. Comparison of OER performance of NiFe-LDH/FeOOH with that of NiFe-based electrocatalysts.

OER catalyst	Electrolyte	η_{100} (mV)	Ref.
NiFe-LDH/FeOOH	**1 M KOH**	**253**	**This work**
	1 M KOH + 0.5 M NaCl	**260**	
	1 M KOH + seawater	**269**	
Ni_2Fe-LDH/$FeNi_2S_4$/NF	1 M KOH	248	6
	1 M KOH + 0.5 M NaCl	250	
	1 M KOH + seawater	271	
N-CDs/NiFe-LDH/NF	1 M KOH	260	7
	1 M KOH + 0.5 M NaCl	285	
	1 M KOH + seawater	340	
NiFe LDH@Co_3O_4/NF	1 M KOH	304	8
	1 M KOH + 0.5 M NaCl	330	
	1 M KOH + seawater	358	
NiMoN@NiFeN	1 M KOH + 0.5 M NaCl	286	9
	1 M KOH + seawater	307	
NiFe LDH/FeOOH	1 M KOH	274	10
	1 M KOH + 0.5 M NaCl	286	
CoP@NiFe LDH	1 M KOH	244	11
	1 M KOH + 0.5 M NaCl	260	
MnO_x/NiFe-LDH/NF	1 M KOH	253	12
	1 M KOH + 0.5 M NaCl	265	
NiTe@NiFe-LDH	1 M KOH	257	13
	1 M KOH + 0.5 M NaCl	277	

Table S3. Fitting parameters for the R_{ct} (Ω) of NiFe-LDH and NiFe-LDH/FeOOH in 1 M KOH, alkaline saline, and seawater, respectively (n=3).

electrolyte	NiFe-LDH	NiFe-LDH/FeOOH
1 M KOH	0.9357±0.0001	0.8760±0.0001
1 M KOH + 0.5 M NaCl	1.0000±0.0002	0.8750±0.0003
1 M KOH + seawater	1.0580±0.0001	0.9316±0.0002

Table S4. Optimum fit parameters for the R_{ct} (Ω) of NiFe-LDH and NiFe-LDH/FeOOH during OER in alkaline saline water, respectively (n=3).

E (V vs. RHE)	NiFe-LDH	NiFe-LDH/FeOOH
1.42±0.01	11.8400±0.0001	11.4400±0.0002
1.47±0.01	2.4470±0.0002	1.7900±0.0001
1.52±0.02	0.9281±0.0001	0.7954±0.0003
1.57±0.03	0.5384±0.0002	0.4898±0.0001
1.62±0.01	0.3590±0.0001	0.3396±0.0001

Table S5. ICP-OES of electrolytes NiFe-LDH and NiFe-LDH/FeOOH after 3 h CP in 1 M KOH + 2.5 M NaCl at a constant current density of 250 mA cm^{-2} stability measurement (n=3).

electrolyte	Ni (mg L^{-1})	Fe (mg L^{-1})
1 M KOH + 2.5 M NaCl	-	-
NiFe-LDH after 3 h	0.189±0.002	0.037±0.003
NiFe-LDH/FeOOH after 3 h	0.006±0.001	0.010±0.002

Table S6. Electrochemical parameters of NiFe-LDH and NiFe-LDH/FeOOH in alkaline saline water and seawater, respectively.

electrolyte	parameters	NiFe-LDH	NiFe-LDH/FeOOH
1 M KOH + 0.5 M NaCl	I_{corr} (10^{-6} A cm^{-2})	10.44	7.50
	E_{corr} (V vs. RHE)	0.90	0.99
1 M KOH + seawater	I_{corr} (10^{-6} A cm^{-2})	18.64	6.27
	E_{corr} (V vs. RHE)	0.87	1.07

References

1 1 G. Kresse, J. Hafner, Ab Initio Hellmann-Feynman Molecular Dynamics for Liquid Metals, *J. Non-Cryst. Solids*, 1993, **156-158**, 956–960.

2 G. Kresse, J. Furthmüller, Efficient Iterative Schemes for Ab Initio Total-Energy Calculations Using a Plane-Wave Basis Set, *Phys. Rev. B,* 1996, **54**, 11169–11186.

3 G. Kresse, D. Joubert, From Ultrasoft Pseudopotentials to the Projector Augmented-Wave Method, *Phys. Rev. B,* 1999, **59**, 1758–1775.

4 J. P. Perdew, K. Burke, M. Ernzerhof, Generalized Gradient Approximation Made Simple, *Phys. Rev. Lett.,*1996, **77**, 3865–3868.

5 S. Plimpton, Fast Parallel Algorithms for Short-Range Molecular Dynamics, *J. Comput. Phys.,* 1995, **117**, 1–19.

6 L. Tan, J. Yu, C. Wang, H. Wang, X. Liu, H. Gao, L. Xin, D. Liu, W. Hou, T. Zhan, Partial Sulfidation Strategy to NiFe-LDH@$FeNi_2S_4$ Heterostructure Enable High-Performance Water/Seawater Oxidation, *Adv. Funct. Mater.*, 2022, **32**, 2200951.

7 P. Ding, H. Song, J. Chang, S. Lu, N-Doped Carbon Dots Coupled NiFe-LDH Hybrids for Robust Electrocatalytic Alkaline Water and Seawater Oxidation, *Nano Res.,* 2022, **15**, 7063–7070.

8 C. Lyu, J. Cheng, K. Wu, J. Wu, N. Wang, Z. Guo, P. Hu, W.-M. Lau, J. Zheng, Interfacial Electronic Structure Modulation of CoP Nanowires with FeP Nanosheets for Enhanced Hydrogen Evolution under Alkaline Water/Seawater Electrolytes, *Appl. Catal., B*, 2022, **317**, 121799.

9 L. Yu, Q. Zhu, S. Song, B. McElhenny, D. Wang, C. Wu, Z. Qin, J. Bao, Y. Yu, S. Chen, Non-Noble Metal-Nitride Based Electrocatalysts for High-Performance Alkaline Seawater Electrolysis, *Nat. Commun.,* 2019, **10** , 5106.

10 K. Jiang, W. Liu, W. Lai, M. Wang, Q. Li, Z. Wang, J. Yuan, Y. Deng, J. Bao, H. Ji, NiFe Layered Double Hydroxide/FeOOH Heterostructure Nanosheets as an Efficient and Durable Bifunctional Electrocatalyst for Overall Seawater Splitting, *Inorg. Chem.,* 2021, **60**, 17371–17378.

11 Z. Zhang, K. Ye, H. Du, X. Li, In Situ Electrodeposition Synthesis of CoP@NiFe LDH Heterostructure as High-Performance Electrocatalyst for Enhanced Seawater Electrolysis, *Int. J. Hydrogen Energy*, 2024, **62**, 722–731.

12 Z. Wang, C. Wang, L. Ye, X. Liu, L. Xin, Y. Yang, L. Wang, W. Hou, Y. Wen, T. Zhan, MnOx Film-Coated NiFe-LDH Nanosheets on Ni Foam as Selective Oxygen Evolution Electrocatalysts for Alkaline Seawater Oxidation, *Inorg. Chem.,*2022, **61**, 15256–15265.

13 X. Ju, X. He, Y. Sun, Z. Cai, S. Sun, Y. Yao, Z. Li, J. Li, Y. Wang, Y. Ren, Fabrication of a Hierarchical NiTe@NiFe-LDH Core–Shell Array for High-Efficiency Alkaline Seawater Oxidation, *iScience*, 2024, **27**, 108736.